ELSEVIER

Journal of Power Sources 76 (1998) 91–97

JOURNAL OF POWER SOURCES

Long cycle life Li–Mn–O defective spinel electrodes

Maria Rita Mancini [a], Lorenzo Petrucci [a], Fabio Ronci [b], Pier Paolo Prosini [c], Stefano Passerini [c,*]

[a] *ENEA, Chemistry Division, C.R. Casaccia, Via Anguillarese 301, 00060 Rome, Italy*
[b] *Chemistry Department, University of Rome I, P.le A. Moro 5, 00185 Rome, Italy*
[c] *ENEA, Energy Division, C.R. Casaccia, Via Anguillarese 301, 00060 Rome, Italy*

Received 3 June 1998; revised 23 July 1998

Abstract

A Li–Mn–O defective spinel phase material has been synthesized through repeated grinding and heating ($T < 400$°C) steps from a mixture of LiOH and MnO_2. The sample has been characterized by X-ray diffraction, thermogravimetric analysis and elemental and oxidation state analyses. At a C/12 charge/discharge rate, the material showed a first-cycle capacity of almost 200 mAh/g that decreased upon cycling to a stable value of 120 mA h/g after the 20th cycle. At a higher rate (C/3.7), the material showed a long cycle life upon lithium insertion/deinsertion with more than 50% of the initial capacity delivered at the 750th cycle. The work was developed within the ALPE (Advanced Lithium Polymer Electrolyte) battery project, an Italian project devoted to the realization of lithium polymer batteries for electric vehicle applications. © 1998 Elsevier Science S.A. All rights reserved.

Keywords: Li–Mn–O defective spinel; Lithium polymer batteries; X-ray diffraction; MnO_2; Long cycle life

1. Introduction

The insertion of lithium in Li–Mn–O compounds was first investigated by Hunter [1], Tackeray et al. [2,3], Goodenough et al. [4], and Tackeray [5]. Since the discovery, several papers and patents have been seen in the past decade [1–12]. Such a wide academic and industrial interest in lithiated manganese oxides for use as cathodes in lithium batteries originates from the major advantages shown by these materials. In fact, although their reversible specific capacities are lower than the theoretical specific capacities of the $LiMO_2$ compounds (M = Co, Ni), they potentially are the lowest cost available cathodic materials for rechargeable lithium batteries. Further, the battery-related industry is well acquainted with the use and manipulation of manganese oxides, i.e., there is a wide range of experience on the handling of these materials. Finally, and perhaps most importantly, manganese oxides are more environmentally safe than other commercially used cathodic materials.

Much of the work performed on manganese oxides is concentrated on the spinel phase ($LiMn_2O_4$) although more recently a large interest has been devoted to the synthesis of layered or amorphous compounds [10–12]. The spinel material can intercalate or deintercalate approximately 1 equivalent of lithium per mol ($Li_xMn_2O_4$, $0 < x < 2$). These processes are accompanied by two distinct structural changes; a cubic–cubic phase transition associated with lithium extraction ($0 < x < 1$) and a cubic–tetragonal phase transition accompanying lithium insertion ($1 < x < 2$). Both processes can be electrochemically driven in the same material by placing it in an electrochemical cell and selecting the appropriate voltage difference with respect to a lithium anode. The first process (Li-extraction) is driven when the cell voltage is slightly above 4 V (4-V plateau) while the lithium insertion process spontaneously proceeds with a cell voltage close to 2.8 V (3-V plateau). In theory, the capacity of both plateaus could be accessed by discharging and charging the cell between 2.5 V (vs. Li) and 4.5 V (vs. Li) with a resulting total capacity of 300 mAh/g of active material. In practice, the reversibility and maximum amount of lithium involved in each of the

* Corresponding author. Corrosion Research Center, Chemical Engineering and Materials Science Department, University of Minnesota, Minneapolis, MN 55455, USA. Tel.: +1-612-625-2335; Fax: +1-612-626-7246; E-mail: passerin@cems.umn.edu

0378-7753/98/$19.00 © 1998 Elsevier Science S.A. All rights reserved.
PII: S0378-7753(98)00144-X

two processes strongly depend on the synthesis conditions used. Highly crystalline materials synthesized at temperatures above 700°C [5] showed a good reversibility over the 4-V process. On the other hand, the same materials showed very poor cycle performance over the 3-V process. This was interpreted as due to the irreversible cubic–tetragonal phase transition, consistent with the onset of the Jahn–Teller effect, when the Mn^{3+}/Mn^{4+} ratio in the material becomes larger than unity [2,3,13]. Spinel phase manganese oxides synthesized at lower temperatures (350–450°C) showed high capacities, good cycling behavior and good rate capabilities in the 3-V plateau. The improvements were ascribed to the defective structure and a reduced crystallinity of the low temperature spinel phase and to the high specific surface area [14,15].

Defective spinels like $Li_2Mn_4O_9$ or $Li_4Mn_5O_{12}$ have been proposed as excellent materials for lithium insertion process over the 3-V plateau [16] on the basis of structural and electrochemical data. $Li_2Mn_4O_9$ was shown to intercalate up to 1.7 equivalents of lithium per mol with only a marginal change in the unit cell volume [14]. Further lithiation induces a tetragonal distortion consistently with the onset of the Jahn–Teller effect, the extent of which is lower than in the pure spinel phase $LiMn_2O_4$. A theoretical capacity of 213 mAh/g and a practical capacity of 160 mAh/g for cycles in the voltage range from 3.3 V to 2.3 V have been, respectively, predicted and demonstrated for $Li_2Mn_4O_9$ but the cycle performance have been demonstrated for only a few cycles [16].

The present work started from this background. The investigations were devoted to the synthesis and the electrochemical characterization of Li–Mn–O defective spinels. The work was initially focused on the selection of the starting materials as well as the optimization of the synthesis conditions. As it will be shown in the following, the work was successful and it enhanced the electrochemical properties of the material in terms of cycle life.

2. Experimental

Li–Mn–O spinel powders were synthesized from LiOH (Carlo Erba) and MnO_2 (Carlo Erba) as starting materials. A stoichiometric mixture of LiOH and MnO_2 (Li:Mn = 1:2) was poured into a tungsten carbide (WC) jar internally coated with polyethylene and mixed by a planetary mill for 6 h with WC balls. Ethanol was used as dispersing medium.

The slurry was dried at 70°C and the resulting powder was heated at 380°C in air for 96 h with intermediate grinding steps. Both the heating and cooling rates were 5°C/min. Powder X-ray diffraction (Cu Ka) was used to ascertain the phase purity of the compounds. The thermal behavior of the obtained material was studied up to 900°C using a Netsch STA 409 thermal gravimetric analyzer in air at a heating rate of 10°C/min. The morphology of the powder was observed by scanning electron microscopy. The specific surface area was determined by a single point BET method using a MICROMERITIC apparatus.

The Li/Mn ratio was obtained by atomic absorption/ICP analysis. The oxidation state of Mn was obtained by wet titration that involved the reduction of manganese to the Mn^{+2} state with an excess of ammonium iron sulfate. The unreacted fraction of the latter was then titrated with potassium permanganate and the oxidation state of manganese was obtained by difference.

The composite cathode used for the electrochemical tests was prepared by mixing the active material with Teflon powder (Du Pont) and carbon (Ketjenblack, AKZO Nobel). The materials were sieved and only the fraction collected from a 400 mesh sieve was used. The materials were dried in inert, dry atmosphere for 24–48 h at 60°C (Teflon), 120°C (carbon) and 150°C (active material). Ten-gram batches of active material (64%), Teflon (30%) and carbon (6%) were mixed by ball-milling for 24 h. To prevent the formation of aggregates in the powders, induced by the absorption of humidity, the materials were handled in dry environments (Dry-box) and/or in sealed containers.

The electrodes were made into pellets (5 mm in diameter) by pressing 12–25 mg of the composite cathode mixture at 3 ton/cm^2. The pellets were dried at 120°C under vacuum for 24 h and placed in two-electrode electrochemical cells in which a 1 M solution of $LiClO_4$ (Fluka, high purity) in propylene carbonate:ethylene carbonate (1:1) was used as electrolyte. The counter electrode was a lithium disc facing the cathode pellet. Glass fiber discs (Whatman GF/A) were used to keep the electrodes separated. The cell stacks were placed in polyethylene cells (Hydraulic T-type connector) flooded with 10–20 drops of electrolyte and sealed. The cells were cathode limited, i.e., the lithium anode was approximately 10–20 times the stoichiometric amount needed by the cathode. The cell were assembled and tested in an M-Braun Dry-box with H_2O and O_2 contents below 1 ppm.

The electrochemical tests were performed by mean of cyclic voltammetry (CV) and galvanostatic charge/discharge experiments. An AMEL voltammetry equipment and a MACCOR Battery Cycler were respectively used to run the experiments.

3. Results and discussion

Fig. 1 shows a high magnification SEM image (10 000 ×) of the surface of a single grain of the synthesized material. The image clearly shows the mushroom-like morphology of the material surface that explains the relatively high surface area (29 m^2/g) measured by single point BET.

Fig. 2 illustrates the diffractogram of the material taken after the thermal treatment (96 h). The main peaks belong

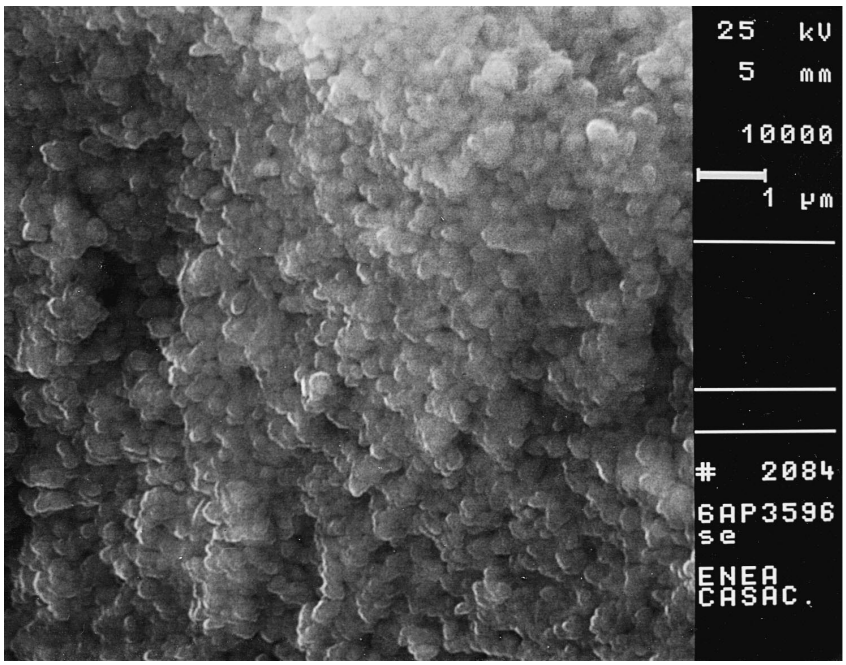

Fig. 1. SEM image of the Li–Mn–O material as obtained after 96 h of thermal treatment at 380°C. The image shows the surface of a single grain magnified 10 000 ×.

to the Li–Mn–O spinel phase but additional small peaks are present, marked by asterisks, most likely associated with the formation of a lithiated γ/β MnO_2 phase as reported by Nohma et al. [17]. From the former set of peaks, the value of the cubic parameter was determined to be 8.15 Å which is lower than the 8.24 Å reported for stoichiometric $LiMn_2O_4$ but near to the 8.16 Å reported for a non-stoichiometric spinel $Li_2Mn_4O_9$ [14].

The thermogravimetric curve reported in Fig. 3 shows a total weight loss of 2.4% in the range 300–700°C. This value is higher than that expected from the completion of the precursor reaction which should result in a maximum weight loss of about 0.8%. On the other hand, it agrees with a thermally induced oxygen loss process of a defective spinel phase formed at low temperature [15,18]. By assuming that the precursor Li/Mn ratio is maintained in the final material, the calculations based on the measured weight loss give a defective spinel with the general formula $Li_{0.95}Mn_{1.90}O_4$. The calculated average Mn oxidation state is 3.71. A chemical analysis of the material (see Section 2) confirmed the conservation of the Li/Mn ratio (0.5) during the thermally-induced synthesis. In addition, the ammonium iron sulfate/permanganate titration also gave an average oxidation state of manganese of 3.71. This value leads to the stoichiometric formula $Li_{0.95}Mn_{1.90}O_4$

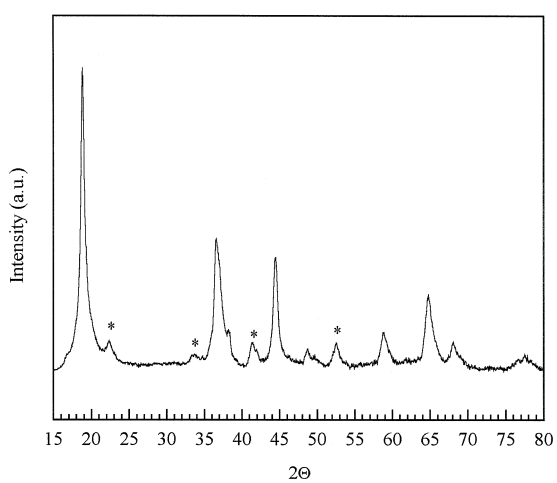

Fig. 2. Powder X-ray diffraction pattern of the Li–Mn–O material as obtained after 96 h of thermal treatment at 380°C. Peaks marked with an asterisk belong to an unknown phase.

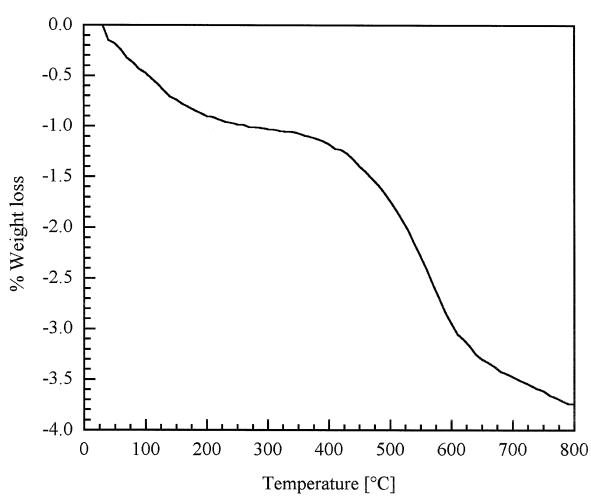

Fig. 3. TGA curve of the Li–Mn–O material as obtained after 96 h of thermal treatment at 380°C.

which is coincident with the stoichiometry obtained by thermogravimetric analysis.

All the results so far reported support a defective spinel phase of the material that can be described by the general formula $Li_{1-\delta}Mn_{2-2\delta}O_4$ with $\delta = 0.05$. This phase belongs to the class of defective Li–Mn–O spinels with varying compositions from $LiMn_2O_4$ ($\delta = 0$) to $Li_2Mn_4O_9$ ($\delta = 0.11$). In spinel notation these defective materials have the cationic arrangement $[Li_{1-\delta\,\square\,\delta}]_{8a}[Mn_{2-2\delta\,\square\,2\delta}]_{16d}O_4$ with vacancies on both the tetrahedral (8a) and the octahedral (16d) sites of the structure [16,18]. On increasing δ, the number of sites available for lithium intercalation increases as does the manganese average oxidation state. This corresponds to an increased capacity of the 3-V discharge plateau and a reduction of the 4-V capacity [16]. Tests performed on the 3-V and 4-V plateaus confirmed the prediction based on the structural data. Fig. 4 shows the voltage behavior of the defective spinel $Li_{0.95}Mn_{1.90}O_4$ during the first cycle discharge at a C/12 rate in the 3-V and 4-V plateaus. The tests were performed on two different cells. To investigate the capacity of the 4-V plateau, the cell was first charged up to 4.2 V. As seen in the figure, the capacity given in the 3-V plateau is almost three times larger than the capacity obtained from the 4-V plateau. Nevertheless, even at a moderately high rate (C/12), the total capacity is 270 mAh/g, i.e., more than 90% of the theoretical capacity. The voltage profiles did not show any sharp transition as expected for a low crystallinity, defective spinel.

On the basis of these promising results, further investigations on the electrochemical behavior of the defective spinel upon cycling over the 3-V plateau were performed. Fig. 5 shows the voltage behavior of a $Li_{0.95}Mn_{1.90}O_4$ composite cathode upon galvanostatic cycling at a C/3.7 rate in the voltage range from 3.4 V to 2.4 V. As seen in the figure, the shape of the charge and discharge half-cycles did show changes upon cycling. From the 3rd cycle, the voltage behavior showed some evidence of a double step during the discharge. Furthermore, the voltage plateaus during the charge and discharge shifted towards higher and lower voltages, respectively, in the initial cycles. Upon cycling, the plateaus moved back toward the original values. The modifications of the voltage at which the intercalation/deintercalation processes take place are best seen in Fig. 6. In the figure, the differential capacity vs. the cell voltage is reported for the initial 15 cycles. In the first cycle, a single cathodic peak (Li-insertion) and a single anodic peak (Li-deinsertion) are seen, respectively, at 2.73 V and 3.03 V. In the second cycle, the cathodic peak is seen to split into two separate peaks and this separation is clearly seen in the third cycle. The new cathodic peak, centered at a lower voltage, became the only peak in the fourth and fifth cycles. On cycling, its position stabilized at about 2.6 V. From the sixth cycle, the original cathodic peak ($V^{c}_{peak} = 2.73$ V) appears again in the differential capacity vs. voltage plot and it grew in intensity in the following cycles. On the anodic side of the plot, the anodic peak is seen to shift towards higher voltages in correspondence with the formation of the new cathodic peak. As a further confirmation of this correlation, the anodic peak moved back towards its initial position when the intensity of the new cathodic peak decreased. Finally, after 15 cycles, again a single cathodic peak and a single anodic peak are seen in the differential capacity vs. voltage plot. Although they appear to be broader than the original peaks, the voltage values are equal ($V^{c}_{peak} = 2.73$ V) or only slightly different ($V^{a}_{peak} = 3.10$ V) to the first cycle values. These results seem to indicate some modifications of the crystalline structure of the material. A somewhat

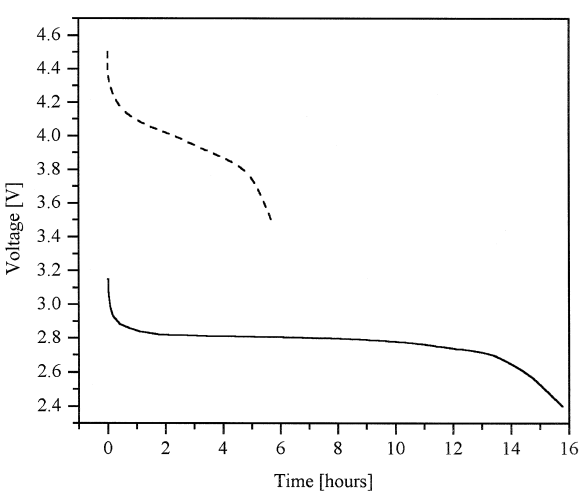

Fig. 4. First discharge curves of $Li_{0.95}Mn_{1.90}O_4$ (composite cathode) in the 3-V (solid line) and 4-V (dashed line) plateaus. Charge/discharge rate: C/12. Counter electrode: Lithium. Electrolyte: 1 M $LiClO_4$ in PC:EC (1:1). Room temperature.

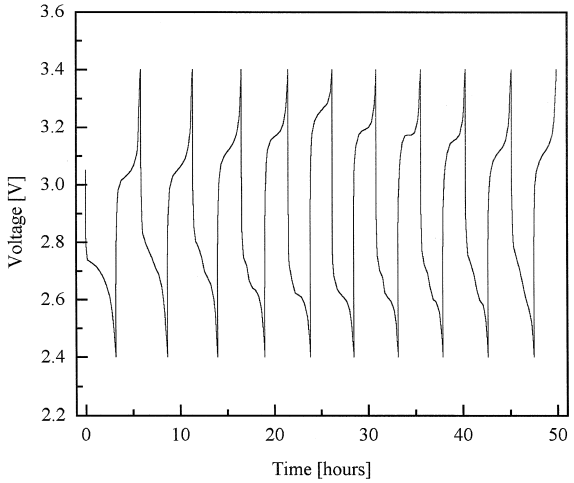

Fig. 5. Voltage behavior upon galvanostatic charge/discharge cycles (initial 10 cycles) of a $Li_{0.95}Mn_{1.90}O_4$ composite cathode in the 3-V plateau. Charge/discharge rate: C/3.7. Counter electrode: Lithium. Electrolyte: 1 M $LiClO_4$ in PC:EC (1:1). Room temperature.

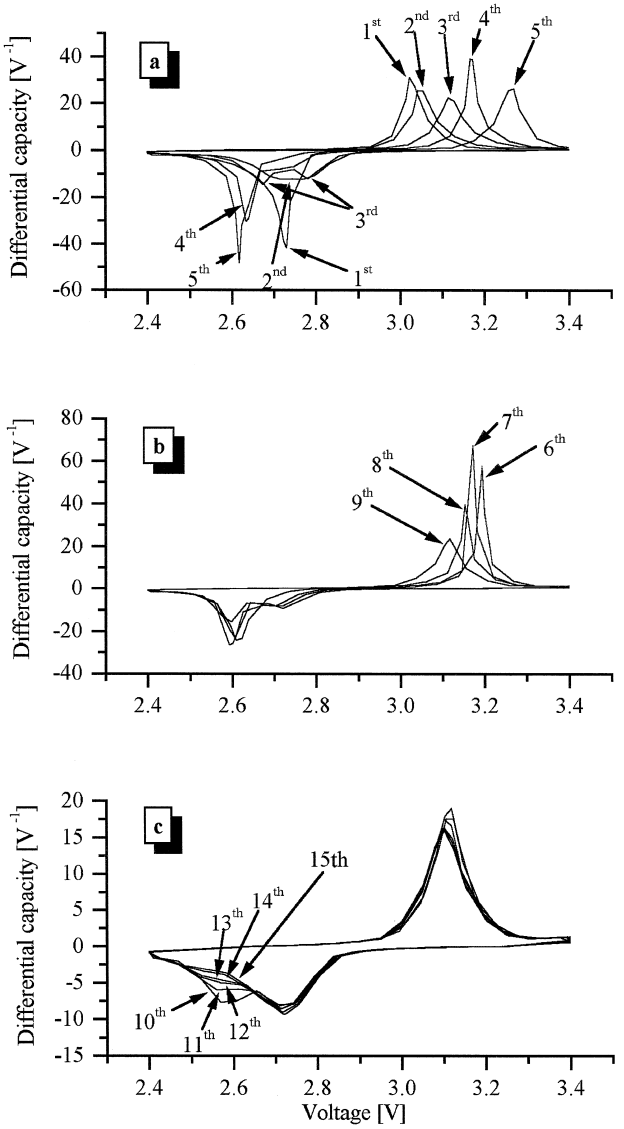

Fig. 6. Differential capacity vs. voltage plots of the charge/discharge of a $Li_{0.95}Mn_{1.90}O_4$ composite cathode in the 3-V plateau. Charge/discharge rate: C/3.7. Counter electrode: Lithium. Electrolyte: 1 M $LiClO_4$ in PC:EC (1:1). Room temperature. The plots were made by manipulating the data reported in Fig. 5.

similar behavior in Li–Mn–O defective spinel has been reported previously [11,16]. The two-stage reaction indicated by the two cathodic peaks (Fig. 6) is consistent with the initial formation of a cubic phase followed by the generation of a tetragonal phase. This latter phase appears toward the end of the discharge when the mean oxidation state of manganese approach 3.5. Nevertheless, the reversibility of the peak position upon initial cycling does certainly support the reversible or non destructive transformation of the defective spinel structure. At the present state, a clear explanation of this behavior is not yet available. An accurate in situ X-ray characterization of the material would be a helpful means of investigating this phenomena.

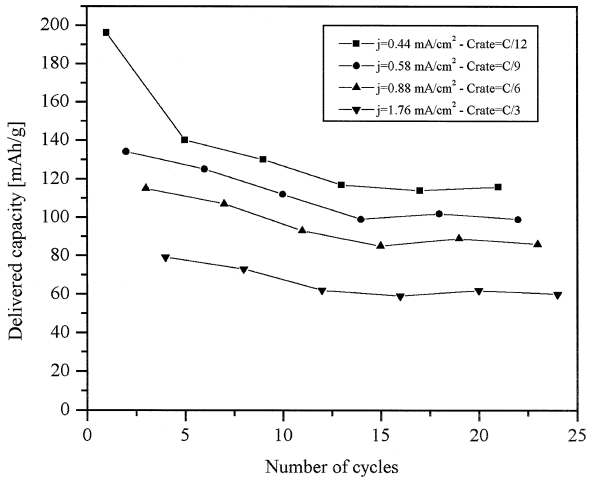

Fig. 7. Delivered capacity as a function of the rate upon cycling of a $Li_{0.95}Mn_{1.90}O_4$ composite cathode in the 3-V plateau. The cell was consecutively discharged at each one of four discharge rates (C/12, C/9, C/6 and C/3). The charge rate was always C/12. The discharge schedule was repeated until stable values of delivered capacity were obtained. Counter electrode: Lithium. Electrolyte: 1 M $LiClO_4$ in PC:EC (1:1). Room temperature.

The cycle rate capability of the material has also been tested. Fig. 7 illustrates the cycling behavior as a function of the charge/discharge rate of a cell containing the $Li_{0.95}Mn_{1.90}O_4$ composite cathode. The test was performed by consecutively cycling the cell in the voltage range between 3.4 V and 2.4 V at four different rates from C/12 to C/3. The cell was always recharged at the lower rate (C/12). The test schedule was repeated six times to reach a maximum of 24 cycles. This test allows for a direct

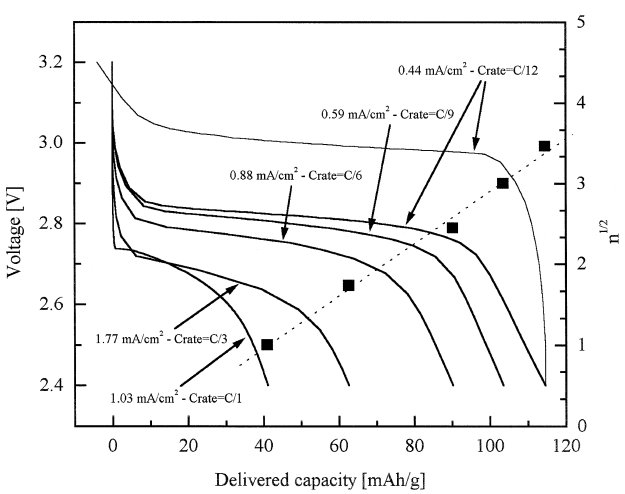

Fig. 8. Voltage behavior during the discharge at different rates of a $Li_{0.95}Mn_{1.90}O_4$ composite cathode in the 3-V plateau. The voltage behavior upon charge at C/12 rate, is also reported. The cycles reported, were selected among the ones with stable values of delivered capacity. The rate vs. delivered capacity correlation is also reported in the figure. Counter electrode: Lithium. Electrolyte: 1 M $LiClO_4$ in PC:EC (1:1). Room temperature.

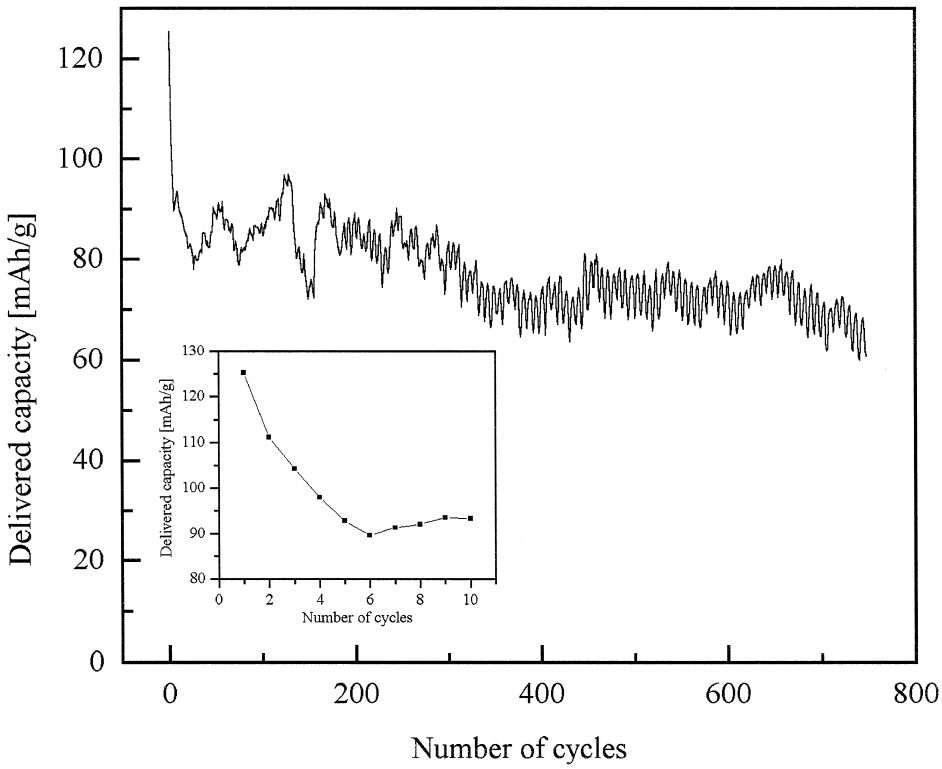

Fig. 9. Long term cycle test of a $Li_{0.95}Mn_{1.90}O_4$ composite cathode in the 3-V plateau. Charge/discharge rate: C/3.7. Counter electrode: Lithium. Electrolyte: 1 M $LiClO_4$ in PC:EC (1:1). Room temperature.

comparison of the rate performance. From the figure it is seen that the delivered capacity decreased during the initial cycles and then stabilized for all four rates of discharge. The voltage behavior upon lithium insertion at different rates and in steady state conditions is illustrated in Fig. 8. The voltage behavior during a standard charge at C/12 rate is also reported. The discharge curves show the characteristic voltage hysteresis in the discharge plateaus (compared with the charge curve), the value of which ranged from 0.20 V at C/12 rate to about 0.35 V at C/1 rate. The delivered capacity as a function of the discharge rate (also reported in Fig. 8) was 115, 105, 90, 65 and 40 mA h/g, respectively, at C/12, C/9, C/6, C/3 and C/1 rate. The linear correlation shown by the delivered capacity as a function of $n^{1/2}$ (where n is the denominator in the discharge rate, expressed as C/n, and is inversely proportional to the discharge current) is indicative of diffusion limitations into the active material solid phase [19].

Long term cycle tests were performed on $Li_{0.95}Mn_{1.90}O_4$ composite cathodes upon galvanostatic cycling at a C/3.7 rate. The results are shown in Fig. 9. The delivered capacity is seen to steeply decrease from 125 mAh/g to 90 mAh/g during the initial six cycles (see inset in Fig. 9). After this steep decrease, the cell showed a very modest capacity loss on cycling. After 750 cycles the delivered capacity was about 50% of the first cycle capacity and 77% of the 5th cycle capacity. The capacity fading, from the 5th cycle on, was only 0.03% per cycle. Such a low capacity loss with cycling is a clear indication of a good cycle life for the low-temperature, defective spinel $Li_{0.95}Mn_{1.90}O_4$. In a previous work of Tackeray et al. [16] on the defective spinel $Li_2Mn_4O_9$, it was proposed that the good cyclability of the material was related to the fairly modest lattice expansion (0.3%) upon lithium intercalation up to $Li_{3.7}Mn_4O_9$. The present material showed a somewhat reduced crystallinity (see Fig. 2 and related text) that could enhance the general reversibility of the lithium insertion/extraction process. In addition, a positive effect from the unknown phase impurities present in the material (marked peaks in Fig. 2) cannot be excluded.

4. Conclusions

A Li–Mn–O material has been synthesized through repeated grinding and heating ($T < 400$°C) steps from a mixture of LiOH and MnO_2. The material, characterized by X-ray diffraction, thermogravimetric analysis and elemental and oxidation state analyses, was identified as a defective spinel phase with a general formula $Li_{1-\delta}Mn_{2-2\delta}O_4$ ($\delta = 0.05$). As a result of the low temperature synthesis (380°C), the material had poor crystallinity and contained a small fraction of a γ/β MnO_2 phase with included lithium. The average oxidation state of manganese in the material was about 3.74. As a result, at C/12 charge/discharge rate, the material showed a first-

cycle capacity of almost 200 mAh/g that decreased upon cycling to a stable value of 120 mAh/g after the 20th cycle. For higher rate (C/3.7), the material showed a long cycle life upon lithium insertion/deinsertion with more than 50% of the initial capacity delivered at the 750th cycle.

Further work is needed to characterize fully the unknown phase present in the active material as well as the structural modifications revealed by the initial lithium insertion/deinsertion cycles. The optimization of the composite cathode composition should also be addressed.

References

[1] J.C. Hunter, J. Solid State Chemistry 39 (1981) 142.
[2] M.M. Tackeray, W.I.F. David, P.G. Bruce, J.B. Goodenough, Mater. Res. Bull. 18 (1983) 461.
[3] M.M. Tackeray, P.J. Johnson, L.A. de Piccioto, Mater. Res. Bull. 19 (1984) 179.
[4] J.B. Goodenough, M.M. Tackeray, W.I.F. David, P.G. Bruce, Rev. Chim. Miner. 21 (1984) 435.
[5] M.M. Tackeray, in: R.J. Brodd (Ed), Progress in Batteries and Battery Materials, Vol. 14, ITE Press, OH, USA, 1995.
[6] L. Li, G. Pistoia, Solid State Ionics, 47, 1991, 231 and 241.
[7] T. Ohzuku, M. Kitagawa, T. Hirai, J. Electrochem. Soc. 137 (1990) 40.
[8] N. Furukawa, T. Nohma, Y. Yamamoto, US Patent 4,956,248, 1990.
[9] R. Koksbang, J. Barker, H. Shi, M.Y. Saidi, Solid State Ionics 84 (1996) 1.
[10] A.R. Armstrong, P.G. Bruce, Nature 381 (1996) 499.
[11] J. Kim, A. Manthiram, Nature 390 (1997) 265.
[12] J.J. Xu, A.J. Kinser, B.B. Owens, W.H. Smyrl, Electrochemical Solid State Letters 1 (1998) 1.
[13] J.M. Tarascon, D. Guyomard, J. Electrochem. Soc. 138 (1993) 2864.
[14] A. de Kock et al., Mater. Res. Bull. 25 (1990) 657.
[15] G. Pistoia, G. Wang Gang, Solid State Ionics 58 (1992) 285.
[16] M.M. Tackeray et al., J. Electrochem. Soc. 139 (1992) 363.
[17] T. Nohma, Y. Yamamoto, I. Nakane, N. Furukawa, J. Power Sources 39 (1992) 51.
[18] R.J. Gummow, A. de Kock, M.M. Thackeray, Solid State Ionics 69 (1994) 59.
[19] D.B. Le, PhD Thesis, University of Minnesota, 1997.